



## Effect of Silylation Hardening on the Electrical Characteristics of Mesoporous Pure Silica Zeolite Film

T. Seo,<sup>a,z</sup> T. Yoshino,<sup>b</sup> N. Ohnuki,<sup>b</sup> Y. Seino,<sup>b</sup> Y. Cho,<sup>a</sup> N. Hata,<sup>b</sup> and T. Kikkawa<sup>a,b,\*</sup>

<sup>a</sup>Research Institute for Nanodevice and Bio Systems, Hiroshima University, Higashi-Hiroshima, Hiroshima 739-8527, Japan

<sup>b</sup>Advanced Semiconductor Research Center, National Institute of Advanced Industrial Science and Technology, Tsukuba, 305-8569, Japan

A pure silica zeolite film was formed by use of hydrothermally crystallized zeolite nanoparticles in a porous silica precursor. The effects of silylation hardening by tetramethylcyclotetrasiloxane (TMCTS) vapor treatment on the electrical characteristics of pure silica zeolite films were investigated. The results from Fourier-transform-IR spectroscopy indicated that the O–H bond decreased by zeolite formation, resulting in the decrease of the leakage current by 1/10. Silylation hardening by TMCTS vapor treatment could reduce the leakage current by 4 orders of magnitude due to the reduction of Si–OH and O–H bonds. The elastic modulus of 5.18 GPa and the dielectric constant of 1.96 were achieved simultaneously by silylation hardening. Consequently, the electrical and mechanical characteristics of the pure silica zeolite film as well as the time dependent dielectric breakdown lifetime were improved.

© 2008 The Electrochemical Society. [DOI: 10.1149/1.3021041] All rights reserved.

Manuscript submitted August 19, 2008; revised manuscript received October 7, 2008. Published November 25, 2008.

With the shrinking of interconnect feature sizes of silicon ultralarge-scale integrated circuits,<sup>1</sup> the signal delay time increases due to the increase of interconnect resistance and parasitic capacitance. To overcome this problem, low-dielectric-constant interlayer dielectric films are needed. Mesoporous silica with pore sizes ranging from 2 to 50 nm have been studied as a potential candidate for ultralow-*k* materials.<sup>2</sup> However, the mechanical strength of the low-*k* film is degraded when mesopores are introduced into the skeletal materials to reduce the film density. Chemical mechanical polishing may cause damage to the porous low-*k* material. Moreover, it is known that the low-*k* film to which mechanical strength is weak receives damage in the packaging, so both low-*k* and high mechanical strength are required. Pure silica zeolite is a promising candidate as an advanced low-*k* material.<sup>3,4</sup> The Young's modulus of the zeolite is 110 GPa,<sup>3</sup> which is larger than that of SiO<sub>2</sub> (73 GPa). This is because the silica network in the zeolite has a three-dimensional crystal structure. The zeolite also has low-*k* because the film density is lower than that of quartz due to the micropores in the crystalline silica. It has a higher elastic modulus, thermal conductivity, and hydrophobicity than SiO<sub>2</sub>.<sup>4-10</sup> The mobile 11 (MEL)-type zeolite was adopted in this work.<sup>11,12</sup> The zeolite was made by a hydrothermal crystallization method. MEL-type zeolite has a 10-membered ring with pore diameters of 0.53 and 0.54 nm as shown in Fig. 1. In this paper, the effects of silylation on the film properties of pure silica zeolite dielectric films are investigated.

### Experimental

The formation process of MEL-type zeolite is shown in Fig. 2. A few nanometers thick native oxide was formed on the surface of Si wafer. First, the precursor solution of tetrabutyl ammonium hydroxide (TBAOH), tetraethyl orthosilicate (TEOS), and ethyl alcohol (EtOH) were mixed and stirred for 24 h at room temperature. Hydrolysis of TEOS was caused by EtOH. TBAOH was purified by filtering with the ion exchange resin. Both TEOS and EtOH were of semiconductor grade. The hydrothermal crystallization method was a synthesis method of zeolite crystal with high temperature and high pressure in water existence. The precursor was heated in an autoclave for 110 h at 100°C. The precursor was then cooled down to room temperature, and heated up again for 10 h at 100°C. The two-stage synthesis is believed to improve the yield for zeolite nanocrystal without changing the particle size.<sup>13,14</sup> The precursor was stirred

during synthesis to prevent agglutination of silica. The suspension prepared by the hydrothermal crystallization method contained zeolite nanoparticles. For comparison, the precursor solution without the hydrothermal synthesis was prepared for porous silica formation.

The porosity of the zeolite was approximately 40%.<sup>6</sup> To reduce the *k*-value, a surfactant was introduced. The concentration of the surfactant to the suspension was controlled from 0 to 9.31 wt %. Butanol and a surfactant of ethylene oxide propylene oxide ethylene oxide triblock copolymer, (EO)<sub>13</sub>(PO)<sub>20</sub>(EO)<sub>13</sub>, were added to the suspension while stirring, so that mesoscopic size pores of several nanometers diameter were formed to reduce the *k*-value of the zeolite film. The zeolite silica film was formed on a Si wafer by spin coating using 2000 rpm for 30 s at room temperature. The film

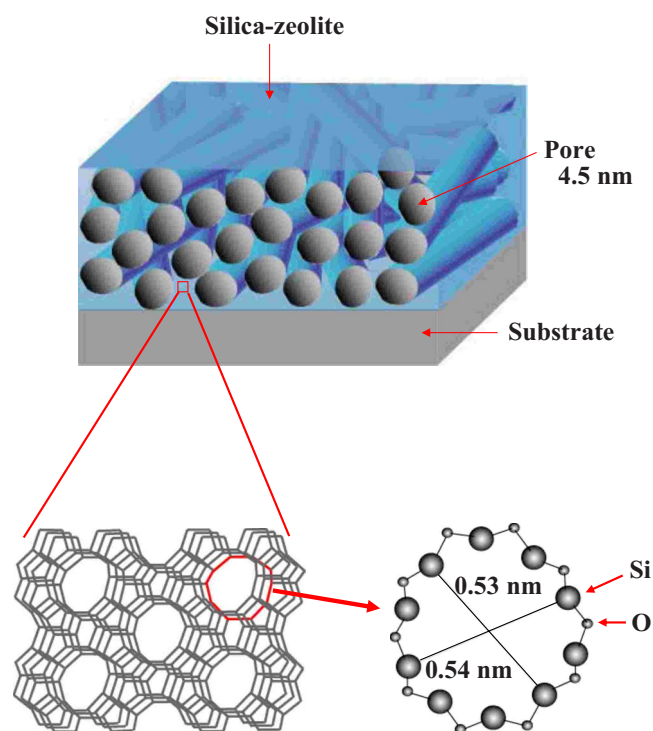


Figure 1. (Color online) A schematic diagram of mesoporous silica low-*k* film and zeolite crystal.

\* Electrochemical Society Active Member.

<sup>z</sup> E-mail: adgsfh1234@yahoo.co.jp

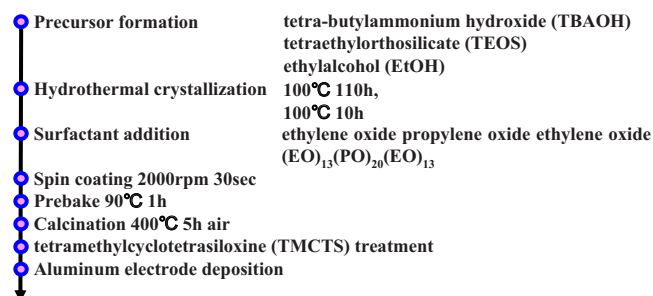


Figure 2. (Color online) Process flow of pure silica zeolite film formation.

thickness could be controlled by the rotation speed of a spinner. After the film was prebaked on a hot plate for 1 h at 90°C, it was calcined at 400°C in air atmosphere. The temperature was 1°C/min. The film was annealed at 400°C for 5 h before being cooled down in air.

The film was treated in the tetramethylcyclotetrasiloxane (TMCTS) atmosphere at 400°C and annealed in the N<sub>2</sub> atmosphere. The gas flow of N<sub>2</sub> was 10 sccm; pressure was 0.8 atm. By this treatment, the pore wall surface was silylated by TMCTS molecules that reacted with Si–OH groups on the pore wall surface as shown in Fig. 3a, and formed the polymer cross-linking network as shown in Fig. 3b.<sup>15</sup>

The effect of silylation was confirmed by electrical, mechanical, and spectroscopic measurements. To measure the dielectric constant of the film, aluminum electrodes with a diameter of 2.0 mm and thickness of 1 μm were deposited on the silica film using a vacuum evaporation system through a stencil mask. The leakage current of pure silica zeolite and porous silica film was measured as shown in Fig. 4a. The dielectric constants of the pure silica zeolite and porous

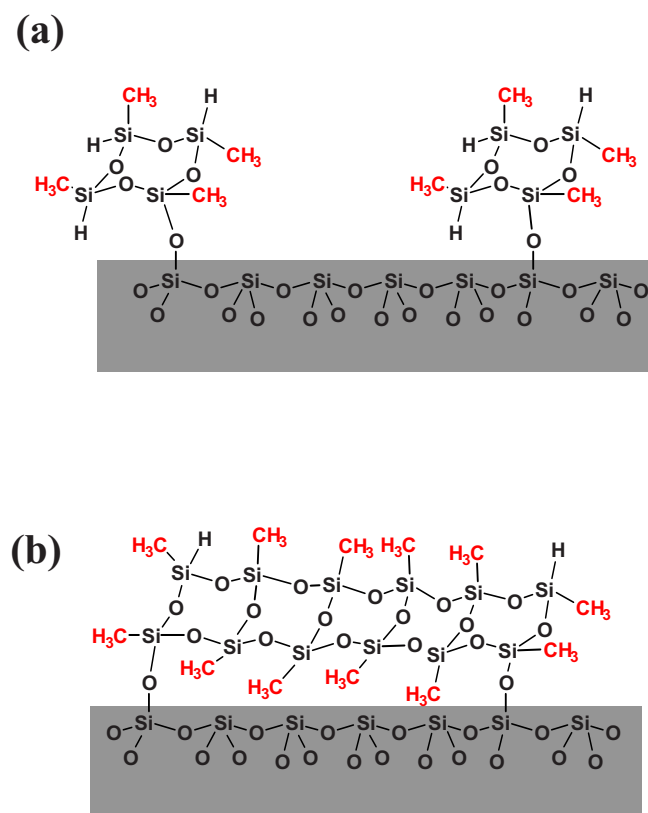


Figure 3. (Color online) Schematic illustration of silylation. (a) Adsorption of TMCTS. (b) Its cross-linking.

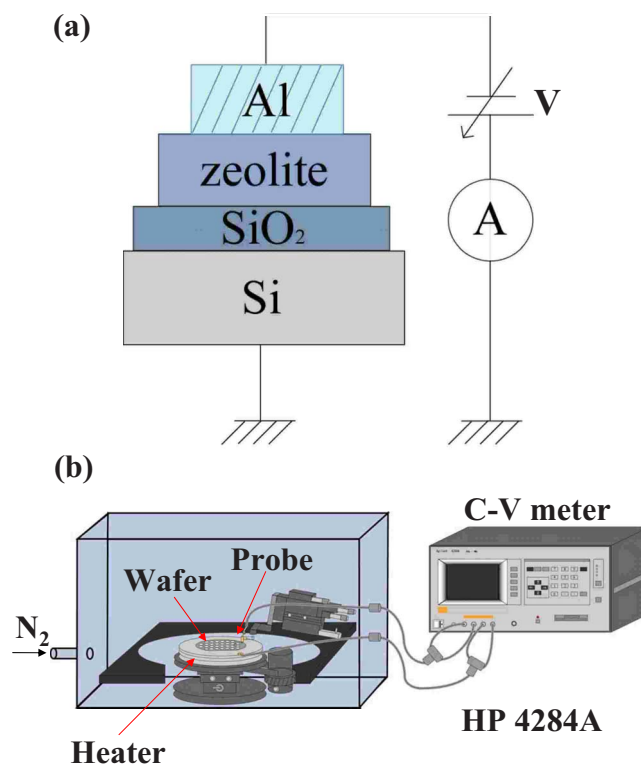


Figure 4. (Color online) Measurement setup for *I-V* and capacitance-voltage characteristics. (a) Wafer-lead measurement. (b) Schematic circuit diagram.

silica film were calculated by measuring the capacitances of metal-insulator-semiconductor structures at 1 MHz as shown in Fig. 4b. The range of the voltage of cyclic voltammetry sweep is 10 V. The zeolite film was baked at 300°C for 2 h in a nitrogen-filled glove box to get rid of adsorbed water. The Si substrate used here was a low-resistance substrate of the p type (100), 0.1 Ω cm. The measurement was carried out at a resolution of 1.0% of relative humidity. The current-voltage (*I-V*) test was measured in the accumulation region. Pore size distribution was calculated by small angle X-ray scattering (SAXS). Measurements of elastic modulus were carried out using nanoindentation.

#### Film Properties

Chemical bonding of pure silica zeolite films was measured by transmission Fourier transform IR (FTIR) spectroscopy. Figure 5 shows a comparison of the FTIR absorbance spectra between pure silica zeolite and porous silica films in vacuum. The existence of zeolite was confirmed by the absorption peak around 560 cm<sup>-1</sup> which is associated with an asymmetric stretching mode of five-membered ring blocks in MEL-type zeolite skeletal.<sup>16</sup> This absorption band was absent in porous silica.

The film thickness and refractive index were measured by spectroscopic ellipsometry. The pure silica zeolite film and porous silica film thicknesses ranged from 210 to 260 nm. The differences of refractive index and porosity on the surfactant concentration of the zeolite film and porous silica film were examined. Figures 6a and b show the dependence of refractive index and porosity on surfactant concentration, respectively. The porosity *x* was calculated by using Lorentz–Lorenz's expression

$$x = 1 - [(n^2 - 1)/(n^2 + 2)] / [(n_{\text{SiO}_2}^2 - 1)/(n_{\text{SiO}_2}^2 + 2)] \quad [1]$$

where *n* and *n*<sub>SiO<sub>2</sub></sub> are refractive indexes of dielectric film and SiO<sub>2</sub>, respectively. The porosities of zeolite and porous silica increased as the surfactant concentration increased. The porosity increased greatly by 4.66 wt % of surfactant concentration, and it saturated in

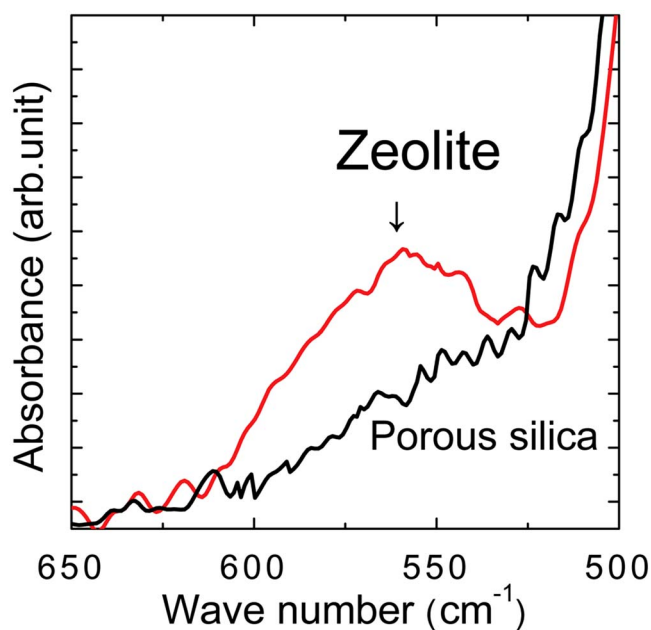


Figure 5. (Color online) FTIR spectra of pure silica zeolite and porous silica films.

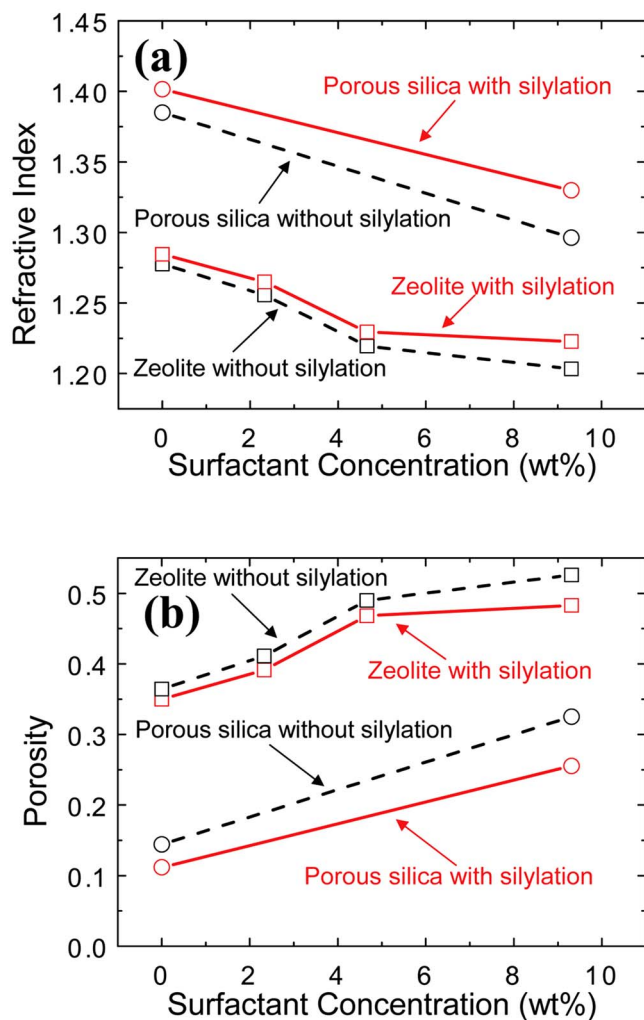


Figure 6. (Color online) Dependence of surfactant concentration for pure silica zeolite and porous silica films with and without silylation. (a) Refractive index vs. surfactant concentration. (b) Porosity vs. surfactant concentration.

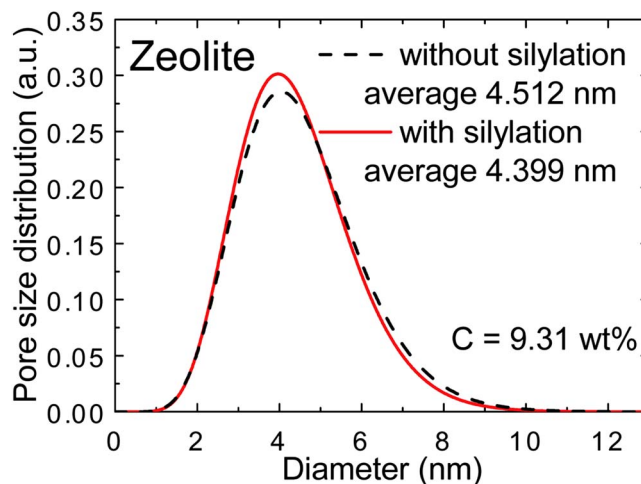


Figure 7. (Color online) Pore size distribution of zeolite films which is 9.31% surfactant concentration with and without silylation.

9.31 wt % of it. The porosity increased up to 52.6% with increasing the surfactant, while it decreased by 10% with TMCTS treatment. Furthermore, the porosity of zeolite is twice as large as that of porous silica.

The pore size distribution was calculated from SAXS measurements. The pore distribution with 9.31% surfactant concentration was confirmed at about 4 nm. However, zeolite micropores around 0.5 nm could not be identified by SAXS. The average pore size increased with increasing surfactant concentration. The increase of the surfactant concentration increased porosity and pore sizes. The decrement of porosity by the TMCTS treatment was understood from porosity and pore size distribution as shown in Fig. 6 and 7. The porosity by the TMCTS treatment was decreased from 4.512 to 4.399 nm, Fig. 7. This is because pore surfaces have cross-linked TMCTS, which practically fill the pores.

FTIR absorbance spectra of zeolite and porous silica films with and without silylation are shown in Fig. 8. The measurements were performed in vacuum to remove the physically adsorbed moisture. A broad absorption in zeolite around  $3513\text{ cm}^{-1}$ , which is associated with the O–H group, was less than that of porous silica film. Both the isolated Si–OH at  $3745\text{ cm}^{-1}$  and the O–H group absorptions were dramatically decreased by the silylation treatment as shown in Fig. 8a. Furthermore, the presence of C–H,  $\text{SiHCH}_3\text{O}_2$ , and  $\text{SiHO}_3$  bonds were exhibited in Fig. 8b, indicating that the film became hydrophobic. Figures 9a and b show dependences of O–H groups and Si–OH groups of zeolite films on surfactant concentrations without silylation and with silylation, respectively. The broad O–H area decreased as the surfactant concentration increased as shown in Fig. 10. Furthermore, the O–H area and the Si–OH area decreased approximately 1/5 by silylation with the TMCTS.

Figure 11 shows that the dielectric constant decreased with increasing surfactant concentration because the O–H area decreased as the surfactant concentration increases, shown in Fig. 10. Pure silica zeolite films show lower dielectric constants than porous silica films. It is thought that the O–H area of the zeolite is smaller than that of porous silica from Fig. 8a. Furthermore, the Si–OH and O–H area decreased dramatically by silylation as shown in Fig. 10, so the dielectric constant decreased from 2.206 to 1.962. Therefore, dielectric constant depends on Si–OH and O–H area.

It is understood that the dielectric constant decreases by the TMCTS treatment, and the elastic modulus and hardness of the pure silica zeolite film increased as shown in Fig. 12. The dielectric constant of 1.96 was achieved with the elastic modulus of 5.18 GPa for TMCTS silylated porous zeolite film. The silylation treatment possibly passivates mechanically weak defects on the pore wall surfaces

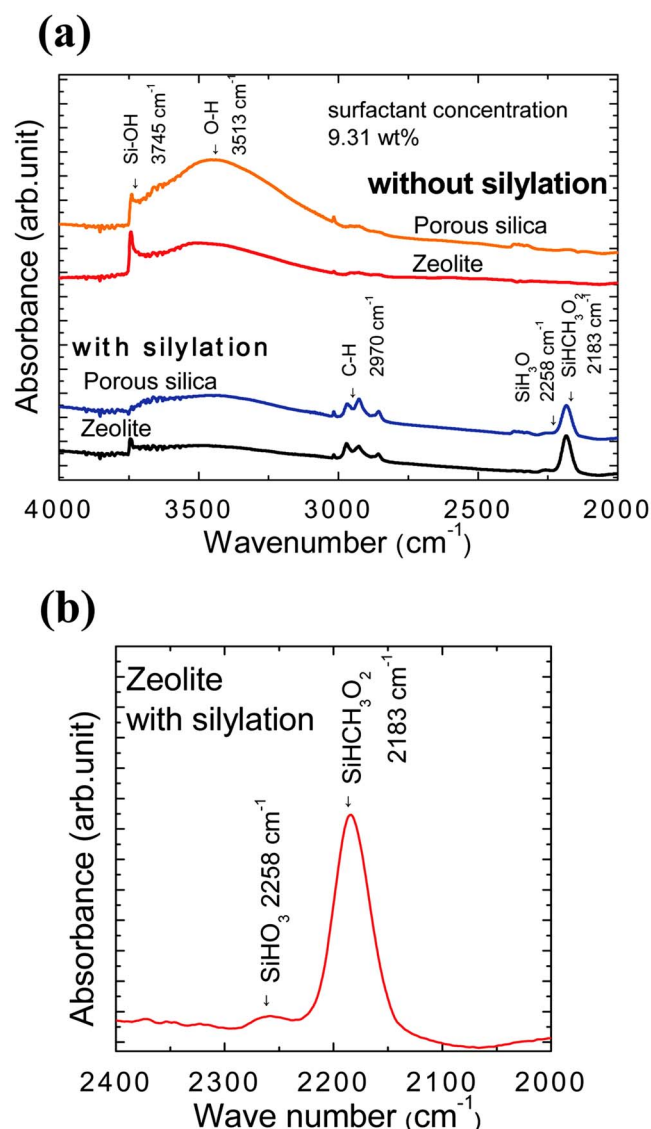


**Figure 8.** (Color online) FTIR spectra. (a) Pure silica zeolite and porous silica films with and without silylation around  $3000\text{ cm}^{-1}$ . (b) Pure silica zeolite film with TMCTS silylation in an expansion scale around  $2200\text{ cm}^{-1}$ .

by forming a polymerized network as shown in Fig. 3. The bridged structure was formed by the TMCTS treatment so that the mechanical strength of the film increased.<sup>15</sup>

#### Electrical Current Characteristic

The leakage current of the pure silica zeolite films was lower than that of porous silica film by 1 order of magnitude and decreased with increasing the surfactant concentration as shown in Fig. 13. The effect on the reduction of leakage current is improved by silylation with TMCTS. The leakage current decreased 4 orders of magnitude at 2 MV/cm. The decrement of the leakage current is attributed to the reduction of OH-related absorption, resulting in a dramatic decrease in the ionic current component.<sup>2</sup> The dielectric constant and leakage current of pure silica zeolite films were lower than those of porous silica films under the present process conditions.

The temperature dependence of leakage current vs electric field was examined in Fig. 14. Figures 14a-d show the temperature dependency of the leakage current vs the electric field with and without silylation for the surfactant concentrations of 9.31, 4.66, 2.33, and 0 wt %.  $J_S$  is expressed in the Schottky emission (SE) model as

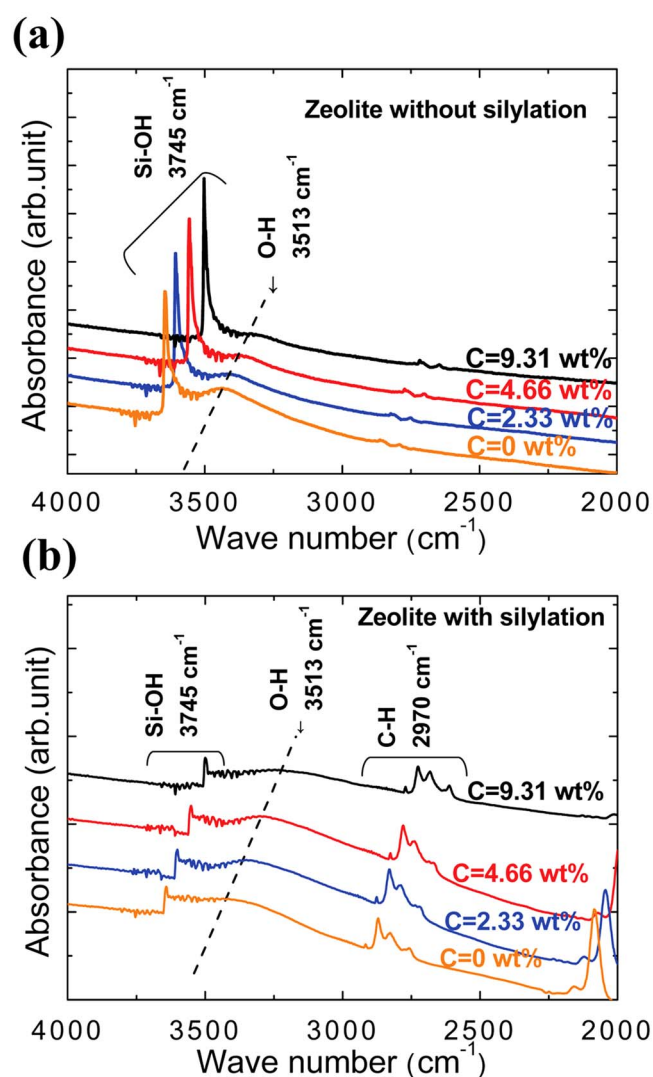


**Figure 9.** (Color online) FTIR spectrum of pure silica zeolite film. (a) Si-OH formation without TMCTS silylation. (b) Si-OH formation with TMCTS silylation.

$$J_S = C_{RD} T^2 \exp\left\{\frac{(\beta_S \sqrt{E} - q\phi_S)/k_B T}{k_B T}\right\} \quad [2]$$

where  $C_{RD}$  is the Richardson–Dushman constant,  $T$  is the absolute temperature,  $E$  is the electric field,  $q$  is the charge of electron,  $\phi_S$  is

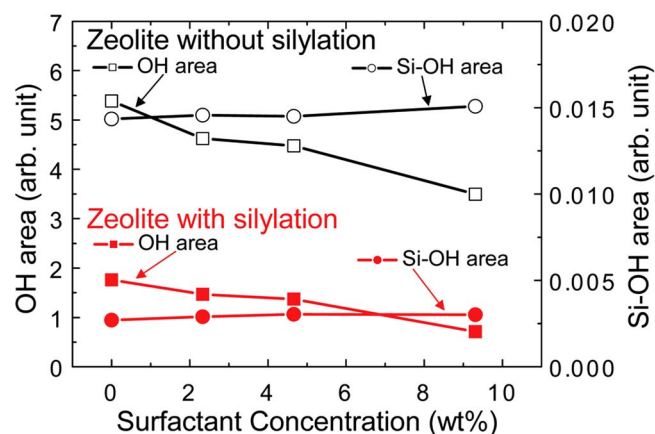


**Figure 10.** (Color online) Dependence Si-OH area and OH area on surfactant concentration with and without TMCTS silylation.

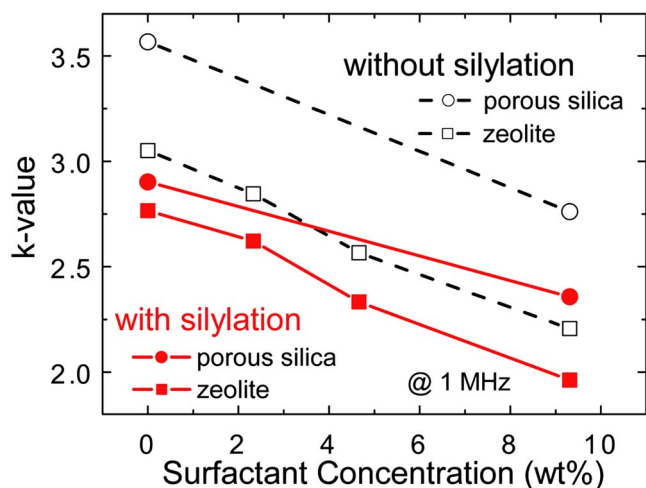


**Figure 11.** (Color online) Dielectric constants vs surfactant concentration for pure silica zeolite and porous silica films with and without TMCTS silylation.

the barrier height,  $k_B$  is the Boltzmann constant,  $\beta_S$  is  $\sqrt{q^3/4\pi\epsilon_0\epsilon_r}$ , where  $\epsilon_0$  is the dielectric constant of air and  $\epsilon_r$  is relative dielectric constant. The leakage current is dominated by the Poole-Frenkel (PF) mechanism,  $J_p$ , which is described as

$$J_p = C_t E^2 \exp\{(\beta_p \sqrt{E} - q\phi_p)/k_B T\} \quad [3]$$

where  $C_t$  is a trap density-related constant,  $\phi_p$  is the barrier height, and  $\beta_p$  is  $\sqrt{q^3/\pi\epsilon_0\epsilon_r}$ . Figures 15a-d show the SE plot for the surfactant concentration of pure silica zeolite with and without silylation, respectively. The slopes of the SE plots are  $\beta_S/k_B T$ . The corresponding PF plots are shown in Fig. 16, and the slopes are determined by  $\beta_p/k_B T$ . A linear slope appeared in the region where these mechanisms are applicable. The linear slope changed around 1.0 MV/cm in the zeolite films without TMCTS treatment as shown in Fig. 15 and 16. The calculated values of  $\epsilon_r$  from SE and PF plots at the electric field of 1.0 MV/cm were 1.49–3.39 and 7.27–53.8, respectively. From spectroscopic ellipsometry, the square of the refractive index  $n^2$  of the zeolite films ranged from 1.44 to 1.65, which was close to the  $\epsilon_r$  of SE, 1.49–3.39. Consequently, the conduction mechanism of the silica zeolite film surpassed 1.0 MV/cm, following the SE model rather than the PF model. The zeolite film with silylation by TMCTS treatment showed neither SE- nor PF-type

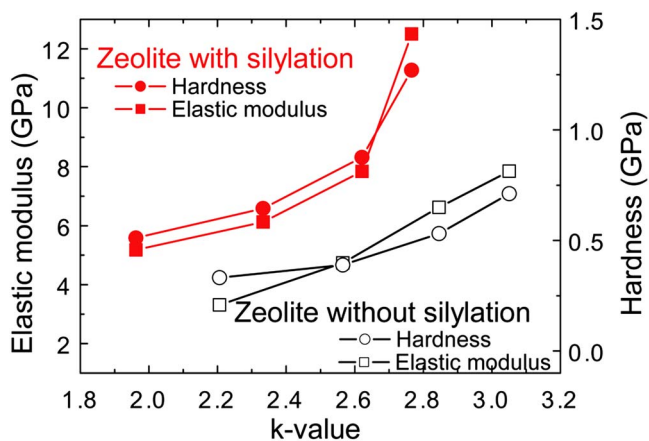


**Figure 12.** (Color online) Elastic modulus and hardness vs dielectric constant for pure silica zeolite and porous silica films with and without silylation.

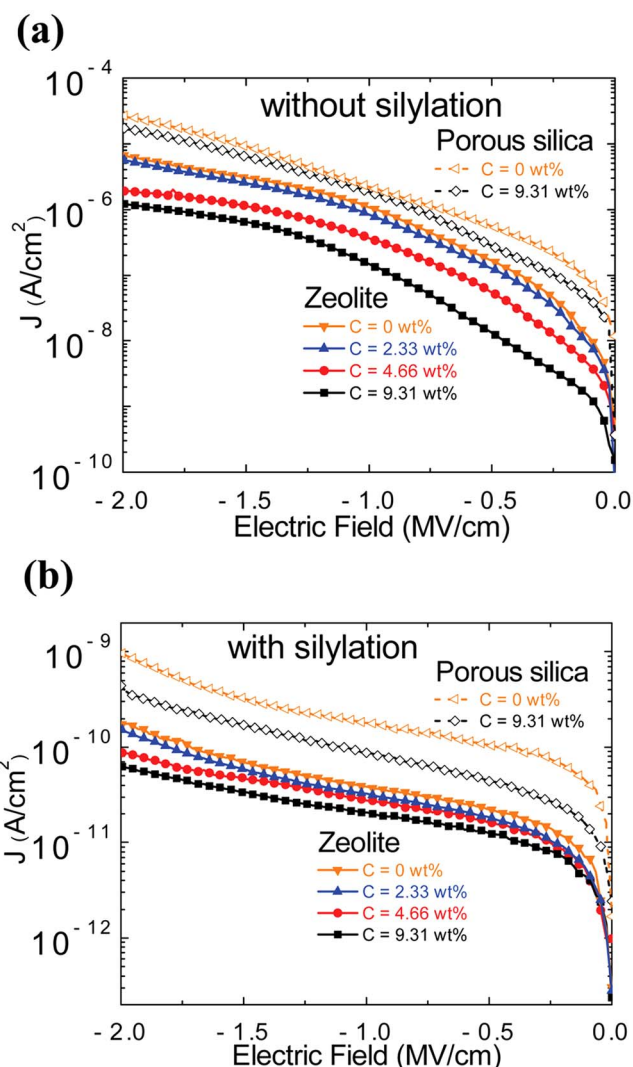


**Figure 13.** (Color online) Leakage current vs surfactant concentration for pure silica zeolite and porous silica films. (a) With TMCTS silylation. (b) Without TMCTS silylation.

conductions below 1.5 MV/cm. The slope changed around 1.6 MV/cm in the zeolite films with TMCTS treatment. The zeolite film with silylation by TMCTS treatment generates an SE-type leakage current when the electric field surpasses 1.6 MV/cm. The SE model was confirmed for the TMCTS-treated film only at high electric field. Figure 17 shows an Arrhenius plot of Schottky leakage current as a parameter of electric field. In the low temperature range, the leakage current did not depend on temperature very much so the Schottky mechanism was not dominant. The Schottky barrier height  $\phi_S$  in the temperature range of 110–230°C varied from 0.65 to 1.25 MV/cm as shown in Fig. 18. The Schottky barrier height increased with increasing the surfactant concentration. The O–H area decreases as the surfactant concentration increases, so that the defect density in the zeolite crystal decreases and the Schottky barrier height increases. The increase in the leakage current is attributed to the Schottky barrier height lowering because of increasing O–H area.

Figure 19 shows a Weibull plot for the lifetime of time dependent dielectric breakdown (TDDB) at 3.6 MV/cm. The TDDB lifetime of zeolite film with silylation was improved in comparison with the porous silica film with silylation by a factor of approximately 2.5.

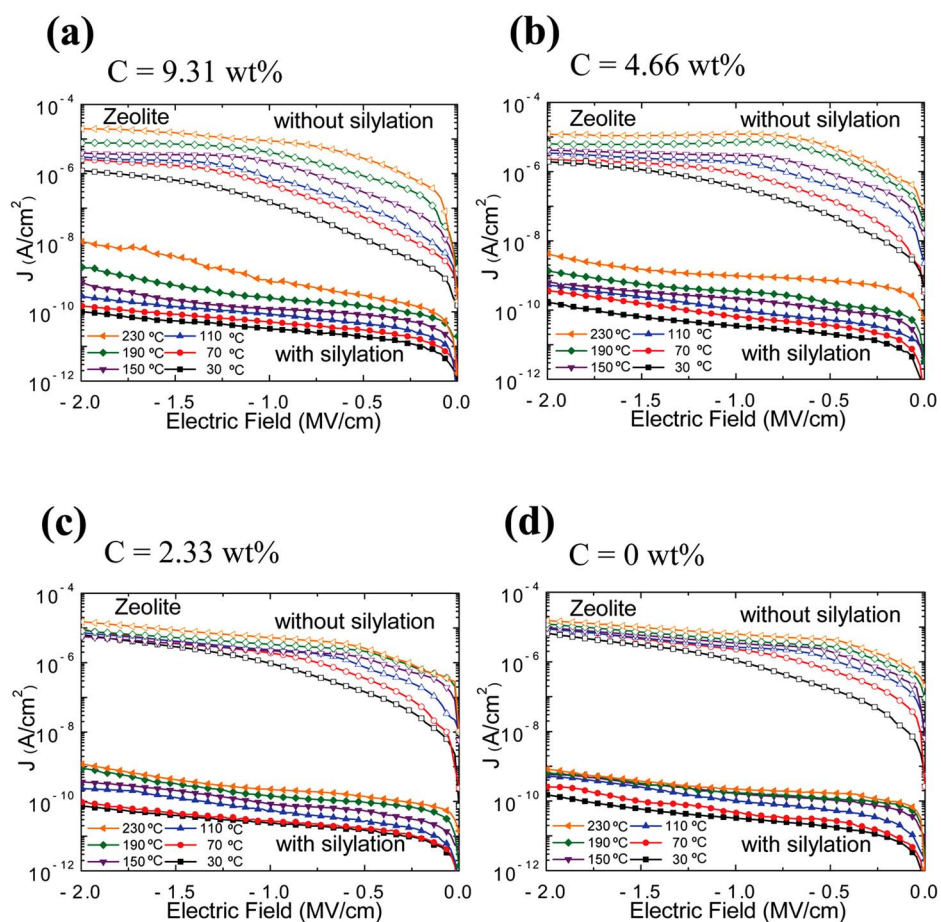


**Figure 14.** (Color online) Dependence of leakage current vs electric field on temperature. (a) Surfactant concentration 9.31 wt %. (b) Surfactant concentration 4.66 wt %. (c) Surfactant concentration 2.33 wt %. (d) Surfactant concentration 0 wt %.

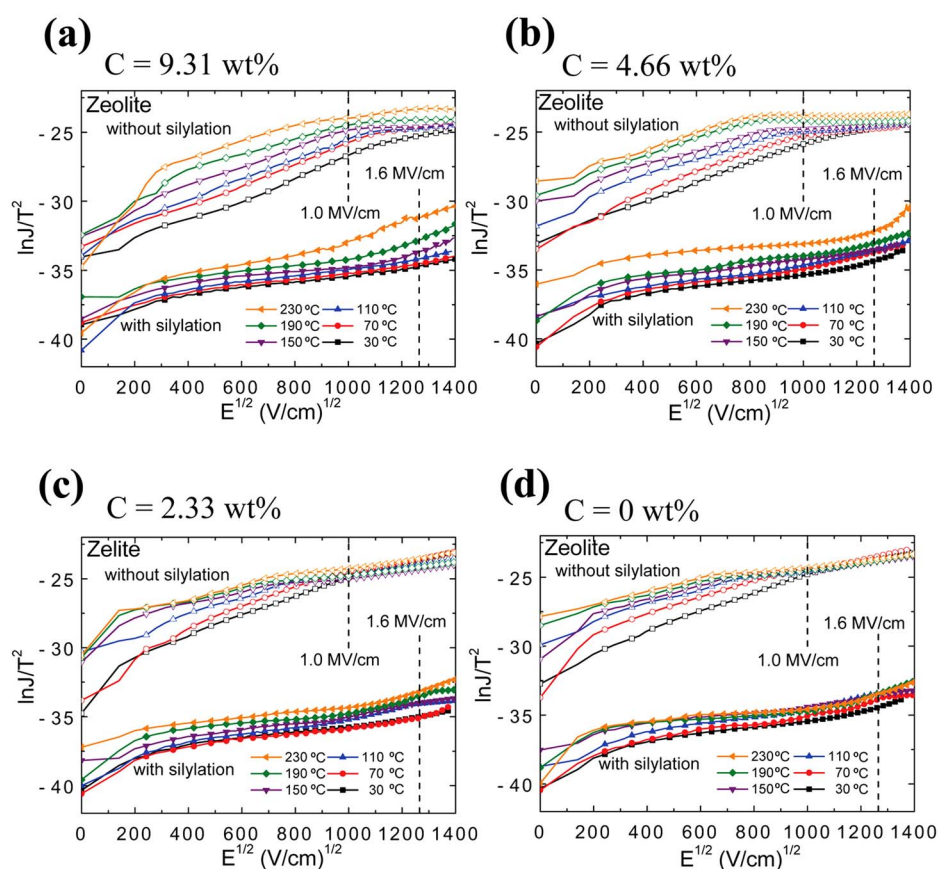


**Figure 15.** (Color online) Schottky plot of silica zeolite films without silylation. (a) Surfactant concentration 9.31 wt %. (b) Surfactant concentration 4.66 wt %. (c) Surfactant concentration 2.33 wt %. (d) Surfactant concentration 0 wt %.

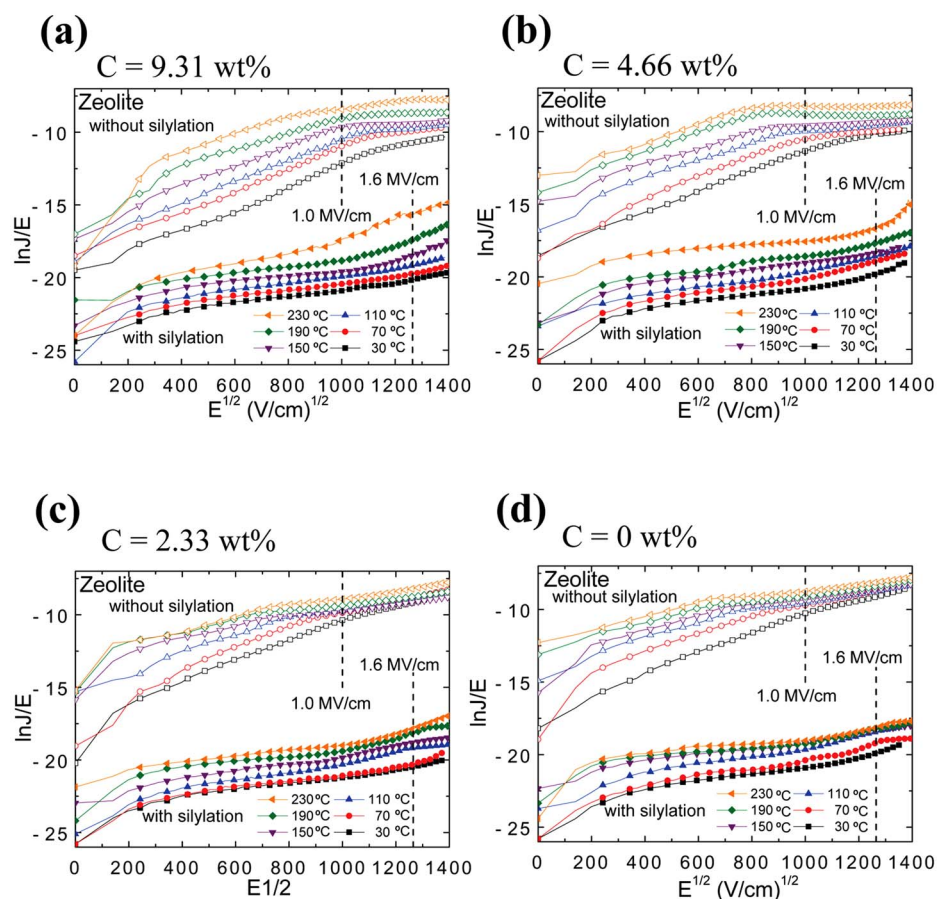


**Figure 16.** (Color online) PF plot of silica zeolite films without silylation. (a) Surfactant concentration 9.31 wt %. (b) Surfactant concentration 4.66 wt %. (c) Surfactant concentration 2.33 wt %. (d) Surfactant concentration 0 wt %.

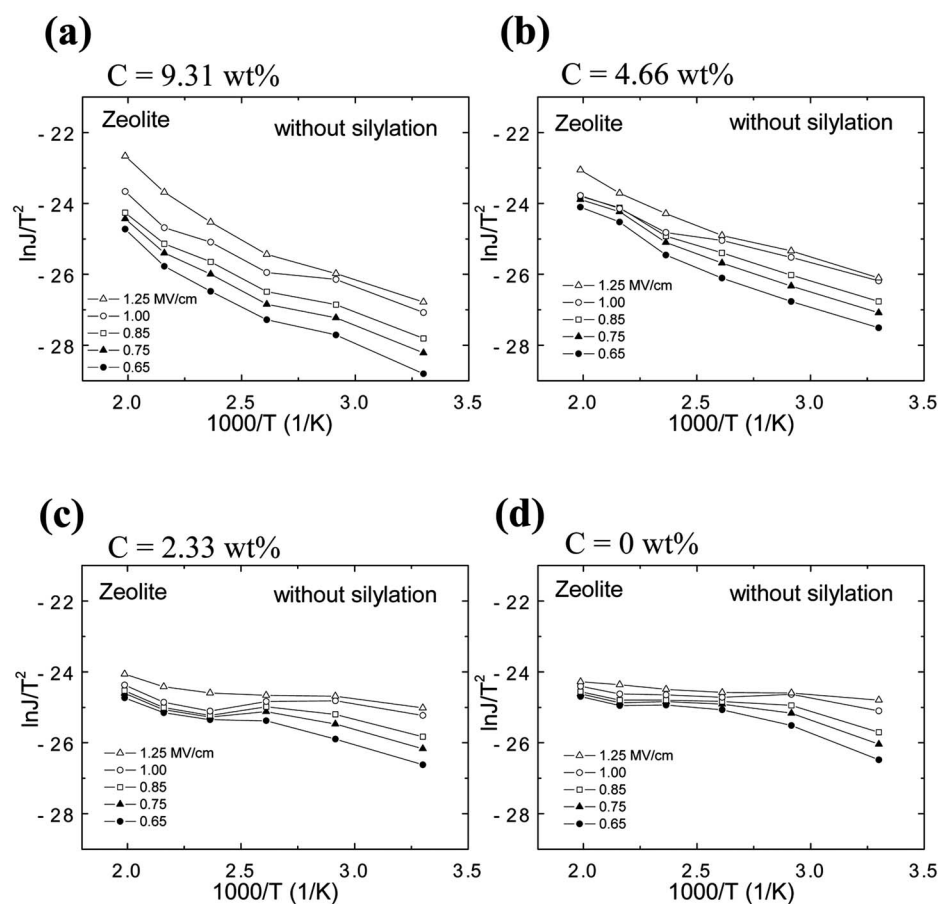


**Figure 17.** Arrhenius plot of Schottky leakage current. (a) Surfactant concentration 9.31 wt %. (b) Surfactant concentration 4.66 wt %. (c) Surfactant concentration 2.33 wt %. (d) Surfactant concentration 0 wt %.

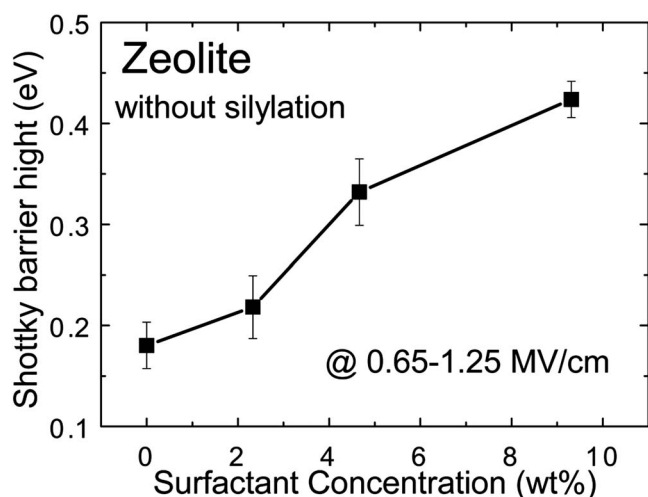


**Figure 18.** Schottky barrier height vs surfactant concentration for pure silica zeolite films without silylation.

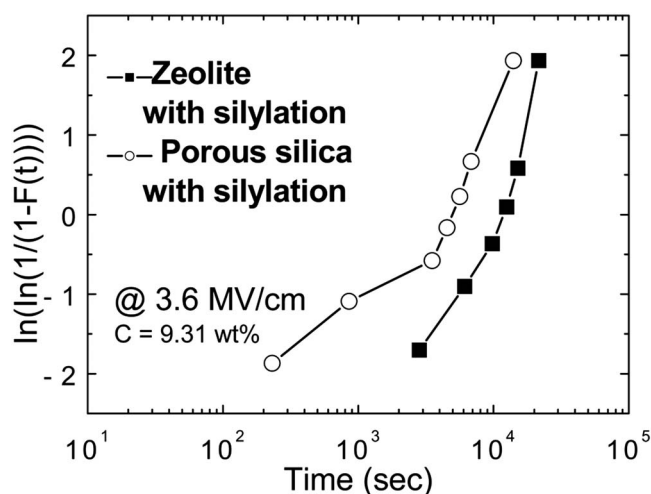


**Figure 19.** Weibull plot of TDDB lifetime at 3.6 MV/cm in 200°C for silica zeolite and porous silica films with silylation.

## Conclusions

The dielectric constant and leakage current of pure silica zeolite film confirming hydrothermally crystallized zeolite nanoparticles were lower than those of a conventional porous silica film. A film containing pure silica zeolite has a dielectric constant of 1.96, an elastic modulus 5.18 GPa, and a leakage current less than  $1 \times 10^{-8}$  A/cm<sup>2</sup> after silylation with TMCTS. The leakage current mechanism of the mesoporous pure silica zeolite film was found to be Schottky emission and the Schottky barrier height increased with increasing the surfactant concentration, resulting in the decrease of the leakage current. The TDDB lifetime of pure silica zeolite film was improved by forming the zeolite crystal in the film. The TMCTS treatment is effective not only for reducing leakage current but also for increasing the mechanical strength of porous zeolite by forming the polymerized network which eliminates water adsorption and passivates defects on the pore wall surfaces.

Hiroshima University assisted in meeting the publication costs of this article.

## References

- H. B. Bakoglu and J. D. Meindl, *IEEE Trans. Electron Devices*, **32**, 903 (1985).
- T. Kikkawa, S. Kuroki, S. Sakamoto, K. Kohmura, H. Tanaka, and N. Hata, *J. Electrochem. Soc.*, **152**, G560 (2005).
- Z. Wang, H. Wang, A. Mitra, L. Huang, and Y. Yan, *Adv. Mater. (Weinheim, Ger.)*, **13**, 746 (2001).
- T. Yoshino, G. Guan, N. Hata, N. Fujii, and T. Kikkawa, in *Extended Abstracts of Solid-State Devices and Materials*, p. 58, Japan Society of Applied Physics, Kobe (2005).
- T. Seo, T. Yoshino, N. Hata, and T. Kikkawa, in *Extended Abstracts of Solid-State Devices and Materials*, p. 462, Japan Society of Applied Physics, Yokohama (2006).
- A. Mitra, T. Cao, H. Wang, Z. Wang, L. Huang, S. Li, Z. Li, and Y. Yan, *Ind. Eng. Chem. Res.*, **43**, 2946 (2004).
- G. Majano, S. Mintova, T. Bein, and T. M. Klapotke, *Adv. Mater. (Weinheim, Ger.)*, **18**, 2440 (2006).
- E. M. Flanigen, J. M. Bennett, R. W. Grose, J. P. Cohen, R. L. Patton, R. M. Kirchner, and J. V. Smith, *Nature (London)*, **271**, 512 (1978).
- Z. Liu, G. Cacciola, G. Restuccia, and N. Giordano, *Zeolites*, **10**, 565 (1990).
- R. A. Van Santen and G. J. Kramer, *Chem. Rev. (Washington, D.C.)*, **95**, 637 (1995).
- S. Mintova, N. Petkov, K. Karaghiosoff, and T. Bein, *Mater. Sci. Eng., C*, **C19**, 111 (2002).
- Z. Li, C. M. Lew, S. Li, D. I. Medina, and Y. Yan, *J. Phys. Chem. B*, **109**, 8652 (2005).
- S. Mintova and T. Bein, *Adv. Mater. (Weinheim, Ger.)*, **13**, 1880 (2001).
- Z. Li, S. Li, H. Luo, and Y. Yan, *Adv. Funct. Mater.*, **14**, 1019 (2004).
- K. Kohmura, H. Tanaka, S. Oike, M. Murakami, N. Fujii, S. Takada, T. Ono, Y. Seino, and T. Kikkawa, *Thin Solid Films*, **515**, 5019 (2007).
- J. Dong, J. Zou, and Y. Long, *Microporous Mesoporous Mater.*, **57**, 9 (2003).